PCCP

ROYAL SOCIETY OF CHEMISTRY

PAPER

View Article Online
View Journal | View Issue

Cite this: *Phys. Chem. Chem. Phys.*, 2025, **27**, 18635

Plasmonic degradation of plastics on gold nanoparticles: electronic-scale insights from computation

Hajar Hosseini, Connor J. Herring, Noshir S. Pesika and Matthew M. Montemore *

The growth in demand for plastic products in our rapidly industrializing society has led to a surge in global plastic production. Plasmonic nanostructures can harness light energy for catalytic reactions, presenting a promising avenue for catalyzing plastic degradation. Through real-time, time-dependent density functional theory (RT-TDDFT) simulations, we find that plasmonic systems can significantly enhance photodegradation of polymers and we study the mechanism of plasmon-driven photodegradation. We first benchmark our methods by studying gas-phase monomers and achieve qualitative agreement between our methods and what is experimentally known: the gas-phase monomers react significantly to an applied field (*i.e.*, light) only for photosensitive polymers. We next find that gold nanoparticles can significantly enhance the degradation of both photosensitive and non-photosensitive monomers and oligomers. Interestingly, if any part of the oligomer is near the nanoparticle, the entire oligomer degrades, indicating that the degradation may be relatively long-ranged on the molecular scale. We also find that charge separation between C and H atoms correlates strongly with photodegradation for polyethylene oligomers.

Received 17th June 2025,
Accepted 12th August 2025

DOI: 10.1039/d5cp02319j

rsc.li/pccp

Introduction

Plastics, being inexpensive, lightweight, and durable, have seen a substantial increase in production over the past 60 years.[1–4] The increased use of plastics, particularly polyolefins, has led to significant disposal challenges in natural environments due to their slow degradation and the reduction of landfill capacity for plastic disposal.[2,5] Thus, plastics pose environmental challenges due to their extended degradation times, with polyethylene estimated to take around 300 years to decompose. Moreover, low-density polyethylene (LDPE), polyvinyl chloride (PVC), and multilayer plastic materials are typically not recycled due to either non-existent or prohibitively expensive recycling technologies. Managing plastic waste is a complex and challenging task, exacerbated by the very low density of plastics, making them challenging to collect and sort efficiently. While plastic contains valuable chemical feedstocks and stored energy, much of its potential is wasted due to improper disposal.[6] These issues underscore the need for society to develop economically viable approaches to tackle the escalating problem of plastic wastes.[7]

Department of Chemical and Biomolecular Engineering, Tulane University, New Orleans, Louisiana 70115, USA. E-mail: mmontemore@tulane.edu

Photodegradation is one potential strategy for plastic degradation. For example, plastics often absorb UV radiation, which can lead to bond cleavage in polymer chains. The wavelength of UV radiation causing plastic destruction, and the degradation efficiency, varies depending on the plastic's composition.[8] Natural photodegradation occurs when sunlight breaks down polymers through photooxidation and direct bond cleavage. This process reduces the molecular weight of the material, causing plastics to become brittle and fragment.[9] To improve photodegradation of plastics, photocatalytic approaches are an area of active research. Overall, the photocatalytic process shows promise as a feasible, cost-effective, and energy-efficient method under mild conditions for mitigating microplastic pollution, with considerable potential for further improvement.[10]

Some photocatalytic technologies have been shown to effectively degrade polymeric materials. Common photocatalysts include TiO_2/Pt, CdS/CdO_x, and CN_x/Ni_2P. However, TiO_2/Pt only absorbs UV light and is expensive, while CdS/CdO_x quantum dots are toxic.[6] Since UV light constitutes just 4% of sunlight, there is a need to develop visible-light-driven,[6,11,12] non-toxic photocatalysts for converting plastics into valuable organic chemicals and/or clean fuels.

Plasmonic systems can be effective photocatalysts for a variety of reactions.[13] Plasmonic nanoparticles strongly interact with resonant photons through the activation of a surface

plasmon resonance, enabling them to focus light within their vicinity.[14–17] This resonance amplifies the light energy around nanostructures, increasing the electric field intensity by up to 1000 times for single particles and in some cases over 1 000 000 times for particles spaced about 1 nm apart.[17] Coinage metal nanoparticles are often used for plasmonic applications, including plasmonic photocatalysis, due to their strong plasmonic response and their stability in many environments.

There has been little work using plasmonic photocatalysis for plastic degradation, and the feasibility and mechanisms are unclear. Metal nanostructures can act as tunable light antennas across the solar spectrum and, when coupled with photocatalyst semiconductors, enhance photocatalytic activity through plasmonic energy transfer.[18] For example, compared to pure $BiOIO_3$, the Ag/AgBr/$BiOIO_3$ composite shows moderately improved photocatalytic activity under UV light (5.4 and 1.1 times better than $BiOIO_3$ and Ag/AgBr) and significantly enhanced activity under visible light (180 and 7.5 times better than $BiOIO_3$ and Ag/AgBr).[19] Similarly, an efficient plasmonic photocatalyst composed of TiO_2 nanobelts/Au nanoparticles showed improved visible light absorption, improved photoelectrochemical response from individual nanoparticles, and higher photocatalytic activity than TiO_2.[20] Ag/AgCl/$SrTiO_3$ photocatalysts were successfully synthesized and showed degradation activity towards target pollutants such as rhodamine B, methyl orange, methylene blue, and phenol and bisphenol A solutions under visible light irradiation, which was attributed to the surface plasmon resonance of Ag/AgCl and efficient separation of photogenerated charges.[21] Additionally, Pt/black TiO_2 photocatalysts with closely spaced but non-bonded Pt species enable efficient, room-temperature, visible-to-near-infrared light-driven alkane dehydrogenation, achieving high turnover numbers and selectivity for various products, far surpassing traditional thermal methods.[22] Similarly, a photothermal catalytic system utilizing Ru/TiO_2 under sunlight or xenon lamp irradiation efficiently converts polyolefin plastic waste into liquid fuels by hydrogenolysis, offering a sustainable recycling solution through solar energy.[23] Given the significant potential of synergistic effects between photocatalysts and the plasmonic phenomenon, further research into their function and degradation efficiency is anticipated to pave the way for advancements in microplastic degradation performance.[18] Since energy can be lost in the energy transfer from the plasmonic material to the semiconductor, using plasmonic materials to directly drive catalysis could be more efficient than using them to sensitize semiconductor photocatalysts. Furthermore, the tunability of plasmonic systems could allow improved efficiency, particularly for visible-light-driven catalysis.

The mechanism behind the plasmon-enhanced photocatalytic process is not yet fully understood because of the complexity of this process.[24] Thus, gaining deeper insight into the mechanisms behind the photocatalytic degradation of plastic-derived chemicals could be key to designing more effective photocatalysts.[6] The distinct characteristics and potential benefits of reaction selectivity observed in plasmonic catalysis could arise from a variety of effects including a localized enhancement of the electromagnetic field, charge carriers, and/or localized heating.[15]

Given the challenges of detailed experimental characterization on the short timescales and length scales most relevant to plasmonic photocatalysis, computation can play a crucial role in elucidating mechanisms. Real-time time-dependent density functional theory (RT-TDDFT) has emerged as a valuable tool for investigating plasmons and other excitations in nanomaterials.[25,26] Its capability to provide clear insight into dynamic processes related to excited states has made it widely utilized. RT-TDDFT, particularly when employing generalized gradient approximation (GGA) functionals, offers a lower computational cost compared to more sophisticated methods and has been shown to give qualitative agreement with experiment.[12,27,28] While experimental systems often involve complex materials and multi-component interfaces, we chose to investigate simpler systems in order to gain clearer mechanistic insights into how plasmonic excitation may drive the initial bond activation steps relevant to polymer degradation.

In this work, we investigated plastic degradation at the atomic and electronic scale by plasmonic gold nanoparticles using RT-TDDFT to gain electronic-scale insights into the mechanism. Gold nanoparticles have been widely studied, including many computational studies, for their catalytic properties,[29,30] but their potential ability to photodegrade polymers has not been computationally evaluated. We conducted an extensive series of calculations to gain detailed insights. We first confirmed that our method can capture trends in photosensitivity of polymeric materials. We then show that gold nanoparticles can greatly enhance the degradation of both photosensitive and non-photosensitive materials. Interestingly, in all cases we studied, degradation occurred throughout the entire molecule rather than being localized to the region near the nanoparticle. We found that charge separation between C and H atoms is a clear signature for degradation of polyethylene oligomers, and our spatial maps of the excitation suggest it is delocalized throughout the molecule. Our tests with various field polarizations suggest that transient charge transfer between the nanoparticle and polymer is important for plasmon-driven degradation.

Computational details

RT-TDDFT computations were conducted utilizing TDAP 2.0[31] which uses localized numerical orbitals as its basis set. Nanoparticles comprising 55 atoms were the primary focus of this work, since our previous studies suggested larger nanoparticles give similar results,[13,32] with adsorbates positioned at the center of the (100) facet of the nanoparticles. Following the methodology of prior studies, the applied electric field was composed of a Gaussian envelope and a sinusoidal component:[13,33]

$$E(t) = \mathrm{A}_0 \mathrm{e}^{\frac{-(t-t_0)^2}{2\sigma^2}} \sin[\omega(t-t_0)]$$

Here, σ, ω, A_0, and t_0 represent the width, frequency, amplitude, and center respectively. The applied field had a frequency of 2.5 eV to 4 eV, a maximum strength of 0.05 Ry bohr^{-1} e^{-1} to 0.4 Ry bohr^{-1} e^{-1} (from 1.29 to 10.28 V $\mathrm{Å}^{-1}$), a Gaussian width of approximately 50 fs and a peak around 40 fs. The time step was

0.5 $\hbar$ Ry^{-1} (0.0242 fs). Unless otherwise specified, the field was applied in all three directions. An optimized double-ζ with single polarization (DZP) basis set was used for the adsorbates, and a double-ζ with two polarization orbitals (DZDP) basis set was used for the gold nanoparticles, except for vinyl chloride where we used the default DZP basis set because of the complexity of the optimization process. The PBE[34] exchange–correlation functional was employed with a mesh cutoff of 150 Ry, and the electronic temperature for Fermi smearing was set to 300 K. Norm-conserving pseudopotentials sourced from ABINIT's Fritz-Haber-Institute pseudo database were employed for all atoms.

The simulation box size was chosen to be big enough for the molecules, which was 25 Å × 25 Å × 25 Å for calculations of monomers in the gas phase and for ethylene and methyl methacrylate on gold nanoparticles; 38 Å × 38 Å × 38 Å for a PMMA oligomer in the gas phase or adsorbed horizontally on gold nanoparticles; and 68 Å × 68 Å × 68 Å for calculations including ethylene oligomers in the gas phase, a PMMA monomer or oligomer vertically adsorbed on gold nanoparticles, and ethylene oligomers adsorbed on gold nanoparticles. The geometries were relaxed and the relaxed configurations were used as the initial state for the excited-state simulations, except for calculations where the nanoparticle-molecule distance was varied.

All simulations were carried out using the PBE–GGA functional due to its favorable computational scaling for large systems and real-time dynamics. While PBE is known to underestimate band gaps and charge-transfer excitation energies, our prior studies on noble metal clusters have shown that PBE-based TDDFT captures the relevant spectral features with reasonable accuracy; for instance, on Au_{55}, PBE-based absorption spectra closely matched experimental results.[13] We performed additional tests on Ag_{20} and Ag_{55} particles and found that our computational setup gave peak energies within roughly 0 to 0.2 eV of the experimental values.[35]

Finally, we note that the applied electric fields in our simulations exceed those used under typical experimental conditions by several orders of magnitude, as discussed in more detail in previous work.[13] These elevated field strengths are common in previous RT-TDDFT work and necessary to access ultrafast dynamics within the simulations, allowing us to observe bond activation events on femtosecond timescales. While such a burst is highly concentrated in time, the energy input itself is not unphysical. Solar intensity is many orders of magnitude lower than our applied fields, while feasible laser intensities[36] correspond to fields only a few orders of magnitude lower in amplitude than our fields. Thus, we focus on trends and fundamental insights rather than quantitatively examining the dynamics. Some previous studies have shown that high fields in RT-TDDFT can lead to qualitative differences from the lower-field regime that is usually of interest for experiments; for example, very strong fields can induce electron emission which is unlikely to occur at all at lower fields.[37] In our simulations, this particular issue is mitigated as we use a localized basis set that does not allow for electron emission. Nevertheless, it is important to be mindful that some care is required when extrapolating from the high-field regime to a lower-field regime. Overall, we expect our key qualitative insights to still inform the design of plasmonic materials and operating conditions in experimental applications.[13,27,28]

Results and discussion

As a test of the suitability of RT-TDDFT with Ehrenfest dynamics for investigating light-driven plastic degradation, we first investigated known photosensitive and non-photosensitive polymers. Specifically, we subjected gas-phase monomers of these materials to light, as represented by an applied oscillating electric field. We tested both a visible frequency (2.5 eV, cyan light) and a near-ultraviolet frequency (4 eV) with a maximum amplitude of 0.1 Ry $bohr^{-1}$ e^{-1}. We then compared our results to previous experimental results on photosensitivity. We consider polymers that naturally degrade in sunlight to be photosensitive.[9]

For these gas-phase calculations, we achieved qualitative agreement between our methods and what is experimentally known, as the gas-phase monomers significantly reacted to the field (*i.e.*, light) only if the polymer is known to be photosensitive (see Table 1). We examined the poly(vinyl ketones)[9,38,39] *tert*-butyl isopropenyl ketone,[40] methyl-isopropyl-ketone, and methyl vinyl ketone, as well as methyl methacrylate,[41,42] as photosensitive monomers, along with ethylene, vinyl chloride, and propylene as non-photosensitive monomers. All were subjected to an electric field in the gas phase. For the photosensitive cases at 2.5 eV, some bond oscillation was seen for methyl methacrylate and methyl vinyl ketone, one bond was broken for *tert*-butyl isopropenyl ketone, and multiple bonds were broken for methyl isopropyl ketone. For all of the non-photosensitive

Table 1 Response of gas-phase monomers to a light pulse (maximum amplitude of 0.1 Ry $bohr^{-1}$ e^{-1}). The experimental photosensitivity of the corresponding polymer is noted in the "photodegradable" column. Here, "dissociation" indicates complete bond breakage

		Electric field	
Monomer	Photodegradable	2.5 eV	4 eV
Methyl methacrylate	Yes	Bond oscillation	Dissociation
Methyl vinyl ketone	Yes	Some bond oscillation	Some bond breakage
Methyl-isopropyl-ketone	Yes	Some bond breakage	Dissociation
Tert-butyl isopropenyl ketone	Yes	One bond breakage	Dissociation
Vinyl chloride	No	Negligible response	Negligible response
Propylene	No	Negligible response	Negligible response
Ethylene	No	Negligible response	Negligible response

cases—ethylene, vinyl chloride, and propylene—there was negligible response. For the 4 eV applied field, the photosensitive materials degraded more strongly than for the 2.5 eV field. However, the trend was the same for both field frequencies: bond activation occurs only when the monomer corresponds to a photosensitive polymer.

We next tested gas-phase oligomers of PMMA (with 5 monomers of MMA) and polyethylene (octadecane) to compare to the gas-phase monomer behavior (*i.e.*, still in the absence of plasmonic gold nanoparticles). Upon exposure to visible light, the oligomers behave qualitatively similarly to the monomers, with the photosensitive PMMA showing much more activation than the non-photosensitive polyethylene (see Fig. 1). This again supports the idea that our computational methodology can correctly capture trends in photoactivation of polymers. Additionally, the oligomers show more activation than the monomers (as inferred from the monotonic increase in bond length at around 45 fs (see Fig. 1(d))), indicating higher photosensitivity. Specifically, the polyethylene oligomer shows some bond oscillation, while the PMMA oligomer shows significant bond breaking.

To test whether plasmonic materials enhance plastic photodegradation, the impact of Au nanoparticles was investigated on the visible-light-induced dissociation of the MMA and ethylene monomers and their oligomers. Our focus is specifically on the initial steps of bond activation, which are expected to be rate-limiting for the relatively inert molecules studied here reacting on Au. Understanding the mechanism of plasmon-induced bond activation provides predictive insight into activation trends. When adsorbed on a Au nanoparticle, the monomers' and oligomers' photodegradation increases dramatically (see Fig. 2 for oligomers). Without Au, the bonds in the ethylene oligomer (decane) increase by less than 0.5 Å (see Fig. 1(c)), but in the presence of Au the bond length increases can exceed 10 Å for C–H bonds and 6 Å for C–C bonds. Similarly, bond activation in PMMA oligomers increases when adsorbed on Au nanoparticles. The C–H bond length extends to over 8 Å, compared to 1.7 Å in the gas phase. Meanwhile, the C–C, C–O, and C═O bond lengths increase to approximately 4 Å, whereas in the gas phase they range from 1.5 to 2.5 Å. Note that we refer to the interatomic distances as bond lengths, even though it is no longer truly a bond once the distance

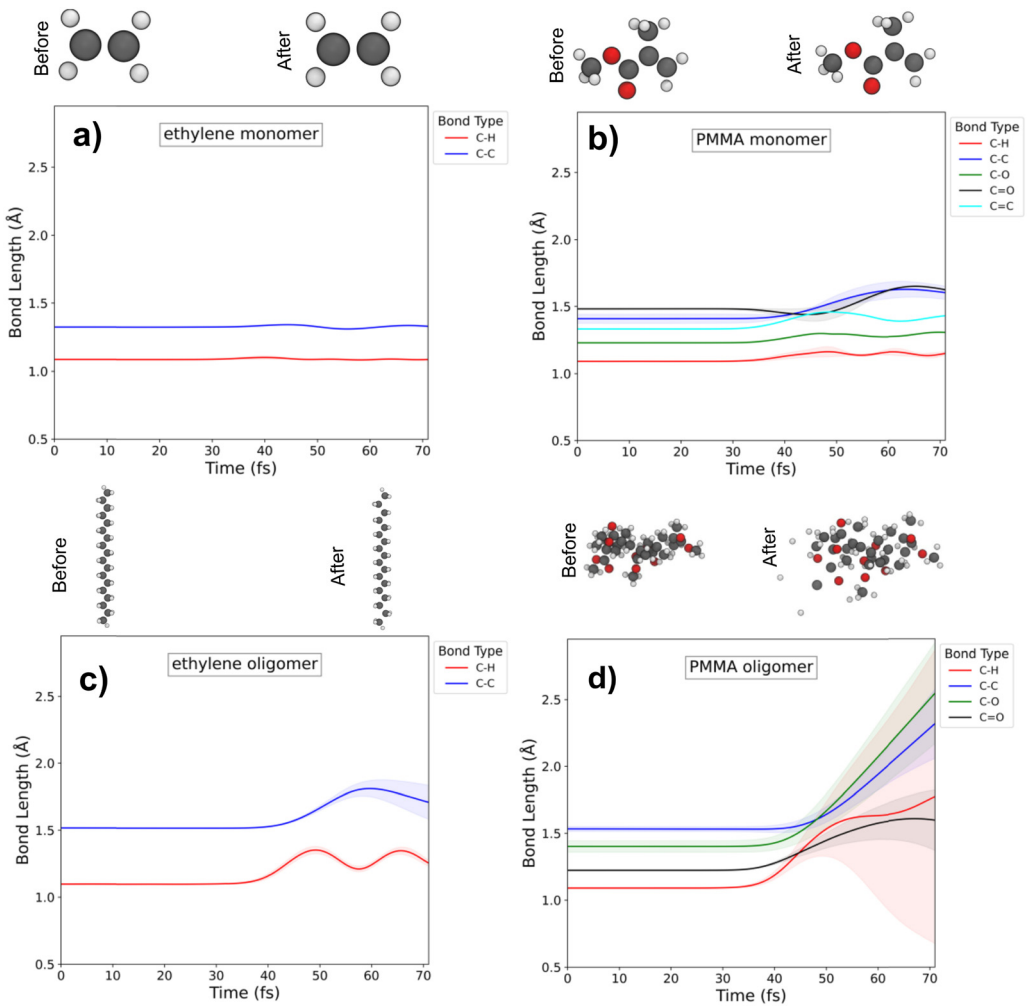

Fig. 1 Average (lines) and standard deviation (shaded regions) of bond length over time for (a) ethylene monomer (b) PMMA monomer (c) ethylene oligomer (d) PMMA oligomer, when applying an electric field in all directions (frequency of 2.5 eV and maximum amplitude of 0.1 Ry bohr^{-1} e^{-1}).

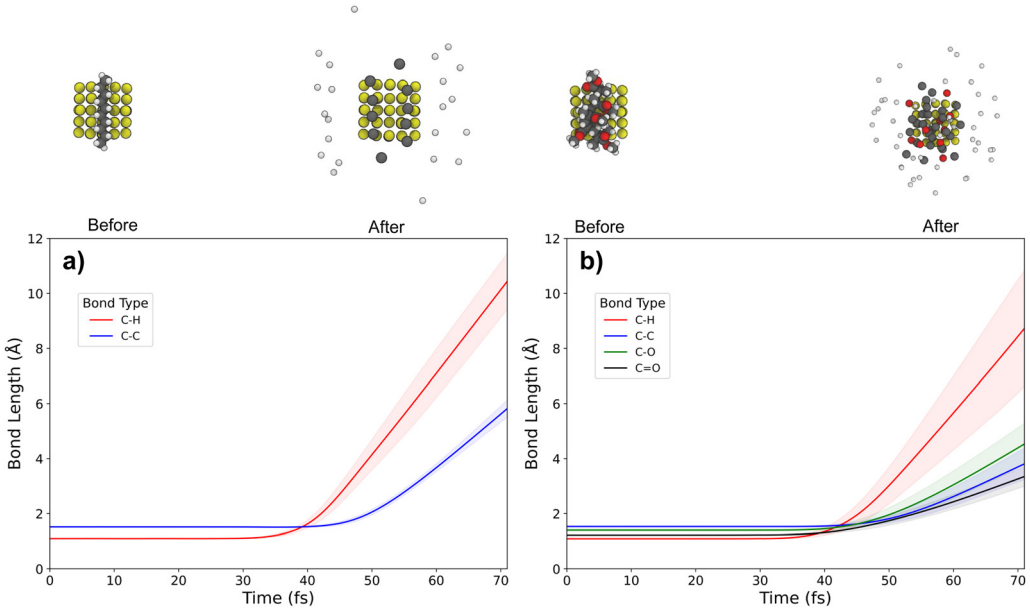

Fig. 2 Average (lines) and standard deviation (shaded regions) of bond length over time for (a) ethylene oligomer and (b) PMMA oligomer adsorbed horizontally on a Au_{55} particle when applying an electric field in all directions (frequency of 2.5 eV and maximum amplitude of 0.1 Ry bohr^{-1} e^{-1}).

exceeds several Å. All of these calculations are performed with a strong field (max amplitude of 0.1 Ry bohr^{-1} e^{-1} which is 2.57 V Å^{-1}), and thus the response is larger than would be expected over this timescale in most experiments. However, these results indicate that plasmonic Au nanoparticles can significantly enhance the photodegradation of both photodegradable and non-photodegradable oligomers. Additionally, the selectivity of bond activation changes somewhat in the presence of the nanoparticles. For the PMMA oligomer in the gas phase, the order is C–O > C–C > C–H > C═O, while when absorbed on Au the order changes to C–H > C–O > C–C > C═O, showing that the nanoparticles were particularly effective in breaking C–H bonds. For the polyethylene oligomer in the gas-phase, C–C and C–H bonds were both activated quite weakly and to a similar degree, while on the Au nanoparticle the C–H bonds were activated more strongly than C–C bonds.

For the calculations discussed thus far, the oligomers were oriented horizontally on the nanoparticle, and the entire molecule decomposes. However, a true polymer would feature regions both near and far from the nanoparticle. To test whether only sections of the molecule near the nanoparticle decompose, we placed both decane and octadecane vertically on a Au_{55} nanoparticle and decane on Au_{79} nanoparticle with an applied a field with a lower maximum amplitude of 0.075 Ry bohr^{-1} e^{-1}(Fig. 3). On both particles, bond activation occurs throughout the entire molecule, with bond breakage observed even for bonds farther from the nanoparticle. For decane, all bonds activate essentially simultaneously, while for octadecane the bonds nearer the surface begin to activate somewhat sooner than bonds farther away. Because the particles behave qualitatively similarly, with C–C bonds in decane reaching ∼2.7 Å *vs.* ∼2.2 Å, we focus on Au_{55} throughout the rest of this work.

To understand the spatial extent of the excitation, we calculated the charge density difference between the nonadiabatic simulation and ground-state calculations along the same trajectory for octadecane on gold. That is, configurations along the nonadiabatic simulation were extracted, ground-state calculations were performed for these configurations, and the charge density was subtracted from the nonadiabatic charge density. This variance in charge density between the non-adiabatic and ground state electron densities at corresponding atomic positions elucidates the nature of the excitation at different points in time.

These calculations (Fig. 4) indicate that the excitation is delocalized throughout the molecule, consistent with the fact that the entire molecule degrades. The excitation tends to be stronger at the ends of the molecule, and especially at the bottom. This is the same pattern as seen in the bond activation.

Because the entire molecule degrades, including bonds far from the surface, a series of calculations involving decane at varying heights above the surface were conducted by re-relaxing the adsorbate-nanoparticle system for the adsorbate at different heights. Subsequently, the system was exposed to the electric field, and the resulting changes in bond length across these different heights are shown in Fig. 5. Increasing the distance of the decane from the gold nanoparticles reduces its degradation, indicating that the end of the oligomer must come in close contact with the Au.

To investigate the mechanisms underlying the nanoparticles' ability to promote dissociation, we examined the charge on the oligomer throughout the simulations *via* Hirshfeld charge partitioning. We focused on the simulations of decane at various heights to examine differences between the cases with strong degradation and the cases with weak or no degradation. For the lowest height, which features the most

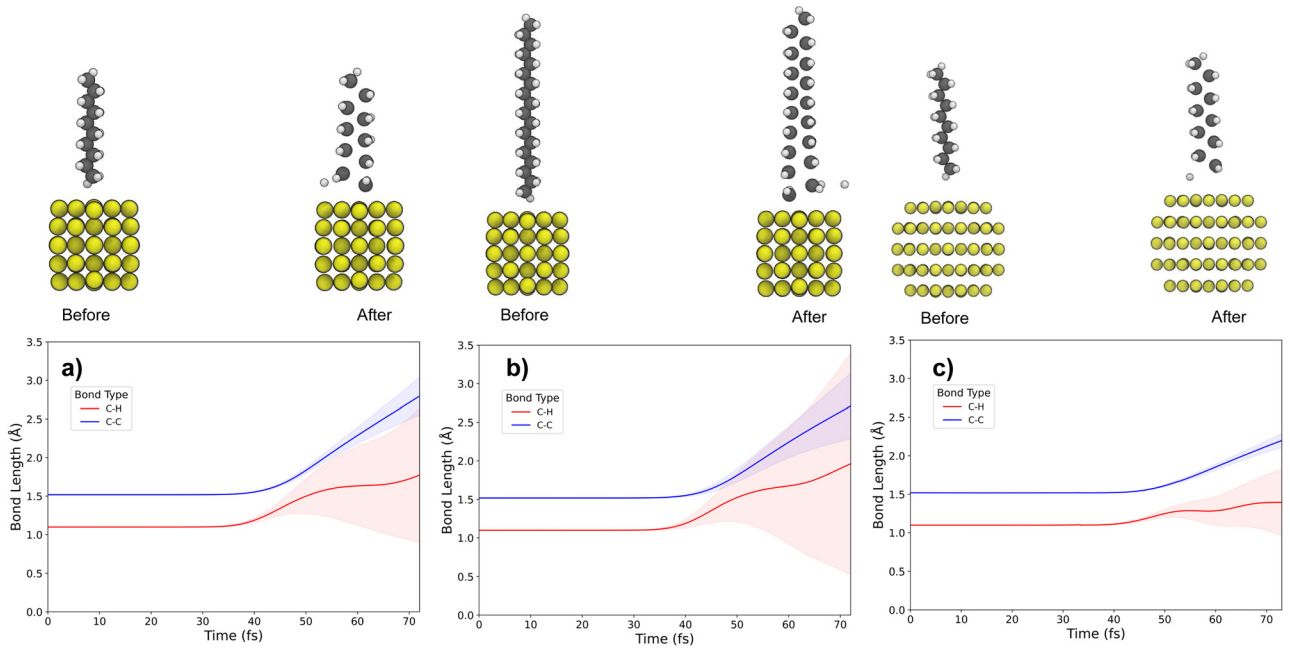

Fig. 3 Average (lines) and standard deviation (shaded regions) of bond length over time for (a) decane vertically absorbed on Au_{55}, (b) octadecane vertically adsorbed on Au_{55} and (c) decane vertically absorbed on Au_{79}, when applying an electric field in all directions (frequency of 2.5 eV and maximum amplitude of 0.075 Ry $bohr^{-1}$ e^{-1}). C–H bonds are depicted in red and C–C bonds in blue.

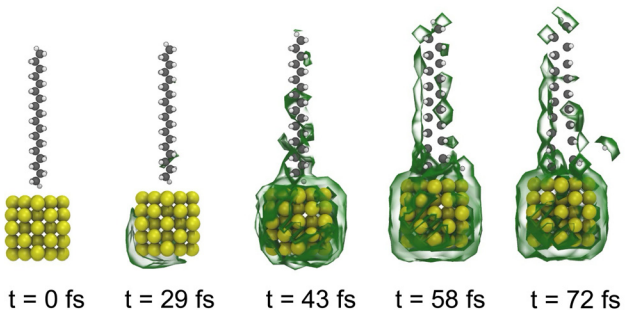

Fig. 4 Charge density difference for octadecane on Au_{55} with the time evolution from left to right. The green isosurface shows excess electrons in the excited state with a value of 10^{-3} e $Å^{-3}$, and the complementary isosurface is not shown for clarity.

degradation, the time-average of the charge on decane stays near 0, indicating only transient charge transfer (Fig. 5(b)). However, fairly large oscillations in the charge are observed. For all larger Au-decane distances, which feature very little bond activation, the charge oscillations are much smaller. At the second height, there is some non-transient charge transfer to the decane, and yet there is still little bond activation. These results suggest that non-transient charge transfer plays little role in bond activation, as we have seen in other plasmonic catalysis systems,[13] but large charge oscillations appear to correlate with degradation.

To further understand charge redistribution throughout the molecule, we examined the charge on C and H throughout the simulation. For times when the electric field is nonnegligible, each atom's instantaneous charge oscillates (see Fig. 6). Overall, oscillation in each atom decreases as the height of the molecule above Au_{55} increases. The atoms that are closest to the surface experience the most oscillation. Qualitatively, the lowest height—the only case exhibiting significant bond activation—differs from other heights in that C atoms develop more positive charges than H atoms (Fig. 6(a)). These results raise the question of whether this charge separation between C and H is a signature for bond activation.

To more comprehensively study the correlation between C–H charge separation and bond breakage, we took the results from a number of calculations, including decane on gold with different amplitudes, heights, and electric field orientations, and octadecane and decane in the gas phase with varying amplitudes and electric field orientations. We calculated the average charge on all H atoms over time and the average charge on all C atoms over time, and took the difference for each bond, and then calculated the average of this value for all bonds in the molecule. We then compared this quantity to the average of the final bond length (at 73 fs) to measure the degree of bond activation (Fig. 7). We find that charge separation between C and H strongly correlates with bond breakage. When there is little or no bond activation (*e.g.*, larger distances from nanoparticles, lower applied field amplitude), the difference in average charges stays slightly positive, near the initial value of 0–0.05 *e*. However, in cases with bond activation, this difference in charges becomes negative, indicating that C becomes more positive relative to H. As this quantity becomes more negative, the bond activation generally increases.

To ensure that the charge separation is not simply a result of bond activation, we also performed a simulation for a case that experienced significant bond activation, but fixed all atoms.

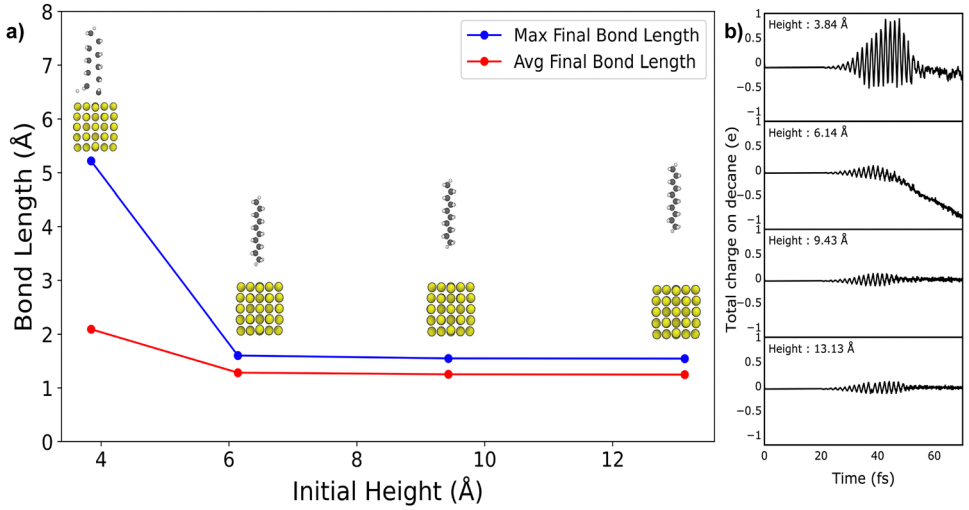

Fig. 5 (a) The final average and maximum bond length at varying adsorbate heights, and (b) change of the total charge on the decane over time for different heights, when applying an electric field in all directions (frequency of 2.5 eV and maximum amplitude of 0.075 Ry bohr^{-1} e^{-1}).

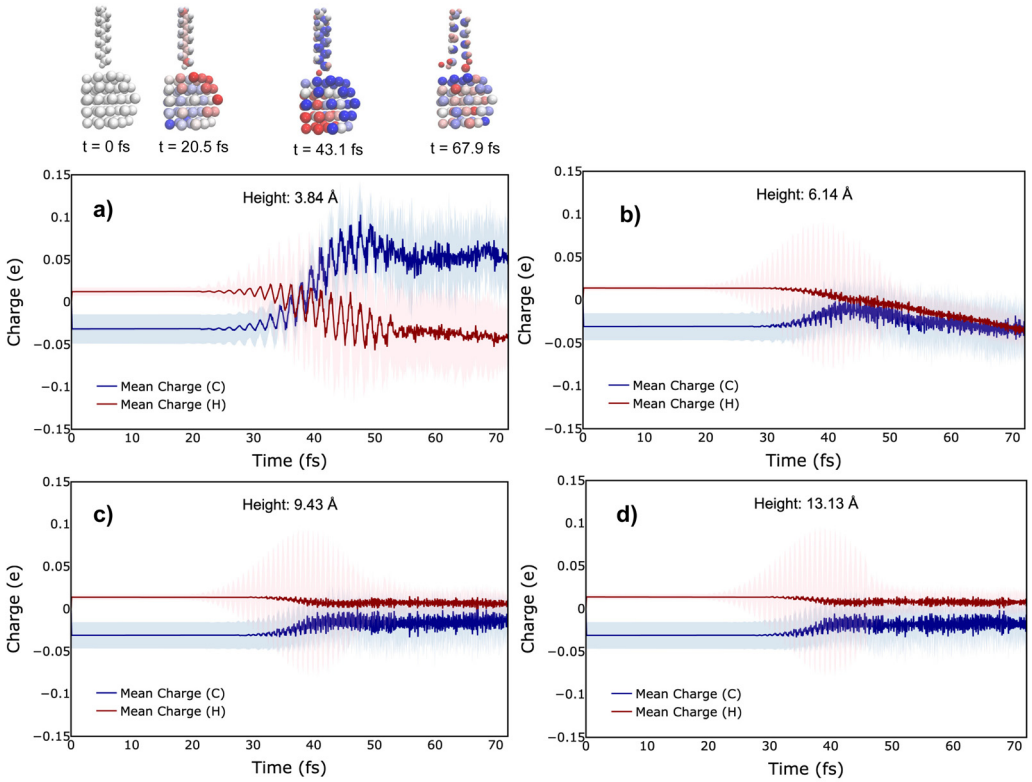

Fig. 6 Change of the charge (relative to initial charge) for each atom in decane over time for different heights increasing from (a) to (d) when applying an electric field in all directions (frequency of 2.5 eV and maximum amplitude of 0.075 Ry bohr^{-1} e^{-1}).

Specifically, we performed a calculation for decane adsorbed on a Au nanoparticle at the relaxed height (3.84 Å) with fixed atoms. Qualitatively, similar charge separation was still observed as in the case with the atoms were allowed to move: C becomes more positive relative to H, although the magnitude was reduced somewhat. This indicates that charge separation is not purely a consequence of bond breakage, but may instead be a driver of bond breakage.

To investigate non-transient charge transfer, we performed calculations for a decane molecule on Au with the field at different polarizations, examining both the total charge on the molecule and the bond activation. Fig. 8 suggests that the transient charge transfer is quite important, and thus that dissociation is not solely a field enhancement effect.

Overall, these simulations were conducted in the gas phase on small particles with strong fields, which may not fully

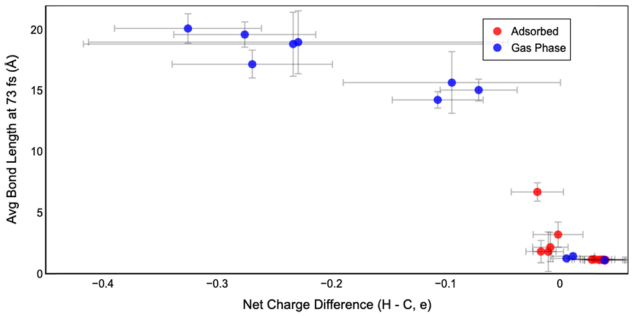

Fig. 7 Average of final bond lengths based on changes of average charges Q over time in each bond when applying an electric field at various amplitudes with a frequency of 2.5 eV. The dots and lines are showing the mean and standard deviation across multiple bonds. Red indicates the oligomer is adsorbed on the Au_{55} cluster and blue indicates the oligomer is in the gas phase.

capture the complexity of real-world catalytic environments. In practical scenarios, solvents or multiple adsorbates may be present and could influence the results. For example, the presence of a solvent could dissipate energy or could be a source of solvated electrons. Thus, while our results provide fundamental insights into plasmon-driven polymer degradation, additional parameters like the solvent (if present), conditions, and particle size could have a significant impact on the efficacy of real-world systems. Nonetheless, our basic demonstration of non-local degradation, where even polymer segments not in direct contact with the nanoparticle become activated, contrasts with typical chemical degradation, which is limited to local interactions. This finding could motivate further exploration into designing high-performance plasmonic systems, such as alloys, to enhance delocalized activation and overall degradation efficiency.

Conclusion

In summary, we utilized RT-TDDFT coupled with Ehrenfest dynamics to investigate light-driven polymer degradation in the gas phase and on Au nanoparticles. We first validated our method on gas-phase monomers in the absence of Au nanoparticles, and were able to reproduce known experimental trends in the photosensitivity of polymers. Au nanoparticles were found to significantly enhance the visible-light-driven photodegradation of both photosensitive and non-photosensitive oligomers, increasing bond activation by more than an order of magnitude in some cases.

We then examined the mechanism underlying plasmon-driven degradation of polyethylene oligomers. Overall, the results suggest that if any part of an oligomer is near the nanoparticle, an excitation will be induced throughout the

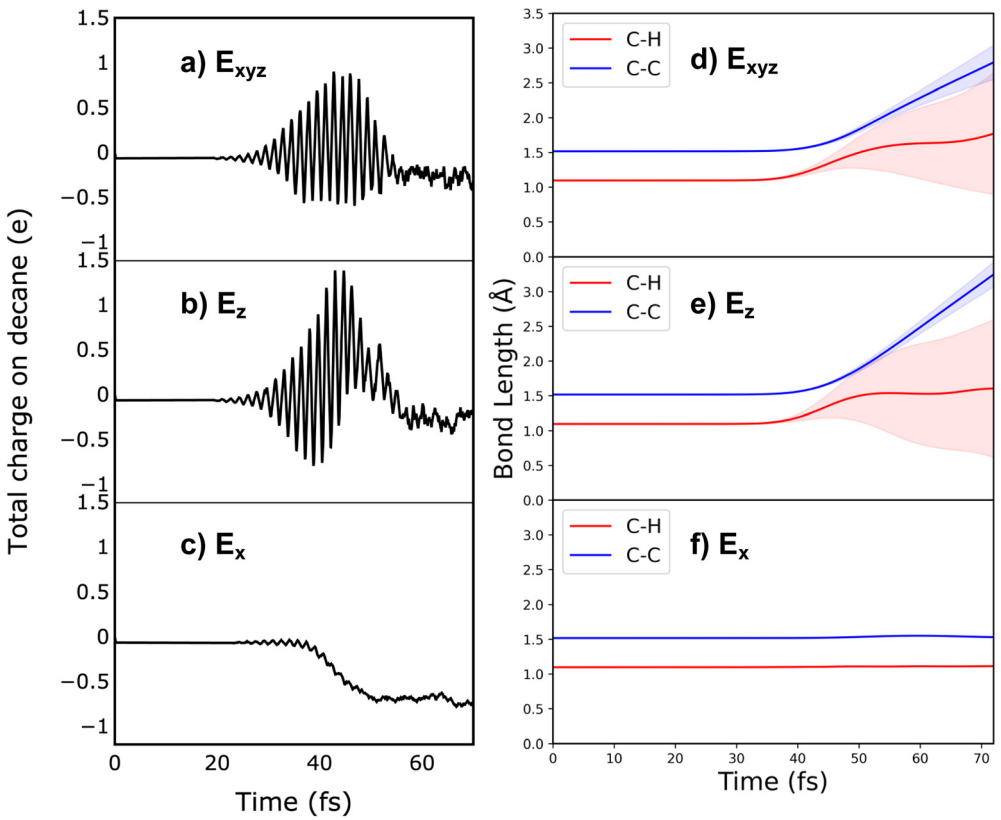

Fig. 8 (a)–(c) Total charge on decane and (d)–(f) average bond lengths with standard deviations over time for decane adsorbed vertically on Au, with various polarizations. The normal direction to the Au particle's surface is the z direction. Applied electric field: frequency of 2.5 and a maximum amplitude of 0.075 Ry $bohr^{-1}$ e^{-1}.

entire oligomer, causing all of it to degrade. This suggests that, to achieve efficient plasmon-driven polymer degradation, it is important for the polymer to come in very close contact with the plasmonic nanostructure (within roughly 4 Å), but the degradation will be relatively nonlocal as compared to the atomic scale. As the system becomes excited, C atoms become positive relative to H atoms, which we find to be a clear signature for bond activation. We also find that transient charge transfer from the nanoparticle to the oligomer facilitates degradation. While our simulations involve simplified, idealized systems, this approach allows us to isolate and understand key atomistic mechanisms that would be difficult to disentangle in more complex, experimentally realistic environments. These insights provide a foundational understanding that can inform more sophisticated multiscale or experimental studies moving forward. These fundamental results serve as a guide to design principles for improving the effectiveness of plasmon-driven polymer degradation.

Conflicts of interest

There are no conflicts to declare.

Data availability

The data underlying this manuscript is available from the authors upon reasonable request.

Acknowledgements

C. J. H. and M. M. M. acknowledge support from the U.S. – Israel Center for Fossil Fuels, administered by the BIRD foundation. H. H. was supported by the National Science Foundation through grant CHE-2154952.

References

1 A. Szyszkowska and D. Galas, Properties, Application and Degradation of Plastics, *Nafta*, 2017, **19**, 20.
2 V. CT, C. Rajagopal, R. Surender, G. Pitchaimari and K. Rajakumar, Development of Photodegradable Environment Friendly Polypropylene Films, *Plast. Polym. Technol.*, 2013, **2**, 22–37.
3 J. Hopewell, R. Dvorak and E. Kosior, Plastics Recycling: Challenges and Opportunities, *Philos. Trans. R. Soc., B*, 2009, **364**(1526), 2115–2126.
4 R. Geyer, J. R. Jambeck and K. L. Law, Production, Use, and Fate of All Plastics Ever Made, *Sci. Adv.*, 2017, **3**(7), e1700782.
5 A. Ammala, S. Bateman, K. Dean, E. Petinakis, P. Sangwan, S. Wong, Q. Yuan, L. Yu, C. Patrick and K. Leong, An Overview of Degradable and Biodegradable Polyolefins, *Prog. Polym. Sci.*, 2011, **36**(8), 1015–1049.
6 Z. Ouyang, Y. Yang, C. Zhang, S. Zhu, L. Qin, W. Wang, D. He, Y. Zhou, H. Luo and F. Qin, Recent Advances in Photocatalytic Degradation of Plastics and Plastic-Derived Chemicals, *J. Mater. Chem. A*, 2021, **9**(23), 13402–13441.
7 A. J. Ragauskas, G. W. Huber, J. Wang, A. Guss, H. M. O'Neill, C. S. K. Lin, Y. Wang, F. R. Wurm and X. Meng, New Technologies Are Needed to Improve the Recycling and Upcycling of Waste Plastics, *ChemSusChem*, 2021, **14**(19), 3982–3984.
8 N. Pandey, B. S. Bohra, C. Tewari, S. P. S. Mehta and N. G. Sahoo, Introduction, Past and Present Scenarios of Plastic Degradation, *Mater. Res. Found*, 2021, **99**, 1–36.
9 P. P. Klemchuk, Degradable Plastics: A Critical Review, *Polym. Degrad. Stab.*, 1990, **27**(2), 183–202, DOI: **10.1016/0141-3910(90)90108-J**.
10 S. H. Paiman, S. F. M. Noor, N. Ngadi, A. H. Nordin and N. Abdullah, Insight into Photocatalysis Technology as a Promising Approach to Tackle Microplastics Pollution through Degradation and Upcycling, *Chem. Eng. J.*, 2023, **467**, 143534.
11 A.-U.-R. Bacha, I. Nabi and L. Zhang, Mechanisms and the Engineering Approaches for the Degradation of Microplastics, *ACS EST Eng.*, 2021, **1**(11), 1481–1501.
12 T. Chen, H. Wang, Y. Chu, C. Boyer, J. Liu and J. Xu, Photo-Induced Depolymerisation: Recent Advances and Future Challenges, *ChemPhotoChem*, 2019, **3**(11), 1059–1076.
13 C. J. Herring and M. M. Montemore, Mechanistic Insights into Plasmonic Catalysis by Dynamic Calculations: O2 and N2 on Au and Ag Nanoparticles, *Chem. Mater.*, 2023, **35**(4), 1586–1593.
14 G. V. Hartland, L. V. Besteiro, P. Johns and A. O. Govorov, What's so Hot about Electrons in Metal Nanoparticles?, *ACS Energy Lett.*, 2017, **2**(7), 1641–1653.
15 Y. Dong, C. Hu, H. Xiong, R. Long and Y. Xiong, Plasmonic Catalysis: New Opportunity for Selective Chemical Bond Evolution, *ACS Catal.*, 2023, **13**(10), 6730–6743.
16 G. V. Hartland, Optical Studies of Dynamics in Noble Metal Nanostructures, *Chem. Rev.*, 2011, **111**(6), 3858–3887.
17 S. Linic, P. Christopher and D. B. Ingram, Plasmonic-Metal Nanostructures for Efficient Conversion of Solar to Chemical Energy, *Nat. Mater.*, 2011, **10**(12), 911–921.
18 M. Golmohammadi, S. F. Musavi, M. Habibi, R. Maleki, M. Golgoli, M. Zargar, L. F. Dumée, S. Baroutian and A. Razmjou, Molecular Mechanisms of Microplastics Degradation: A Review, *Sep. Purif. Technol.*, 2023, **309**, 122906.
19 F. Chen, H. Huang, C. Zeng, X. Du and Y. Zhang, Achieving Enhanced UV and Visible Light Photocatalytic Activity for Ternary Ag/AgBr/BiOIO3: Decomposition for Diverse Industrial Contaminants with Distinct Mechanisms and Complete Mineralization Ability, *ACS Sustainable Chem. Eng.*, 2017, **5**(9), 7777–7791.
20 Q. Chen, H. Liu, Y. Xin and X. Cheng, Coupling Immobilized TiO2 Nanobelts and Au Nanoparticles for Enhanced Photocatalytic and Photoelectrocatalytic Activity and Mechanism Insights, *Chem. Eng. J.*, 2014, **241**, 145–154.
21 S.-F. Yang, C.-G. Niu, D.-W. Huang, H. Zhang, C. Liang and G.-M. Zeng, $SrTiO_3$ Nanocubes Decorated with Ag/AgCl Nanoparticles as Photocatalysts with Enhanced Visible-Light

Photocatalytic Activity towards the Degradation of Dyes, Phenol and Bisphenol A, *Environ. Sci. Nano*, 2017, **4**(3), 585–595.

22 L. Zhang, L. Liu, Z. Pan, R. Zhang, Z. Gao, G. Wang, K. Huang, X. Mu, F. Bai and Y. Wang, Visible-Light-Driven Non-Oxidative Dehydrogenation of Alkanes at Ambient Conditions, *Nat. Energy*, 2022, **7**(11), 1042–1051.

23 Y. Miao, Y. Zhao, G. I. Waterhouse, R. Shi, L.-Z. Wu and T. Zhang, Photothermal Recycling of Waste Polyolefin Plastics into Liquid Fuels with High Selectivity under Solvent-Free Conditions, *Nat. Commun.*, 2023, **14**(1), 4242.

24 Y. Wang and C. M. Aikens, Connectivity between Static Field and Continuous Wave Field Effects on Excitation-Induced H_2 Activation, *J. Phys. Chem. C*, 2023, **127**(31), 15375–15384.

25 L. Yan, F. Wang and S. Meng, Quantum Mode Selectivity of Plasmon-Induced Water Splitting on Gold Nanoparticles, *ACS Nano*, 2016, **10**(5), 5452–5458.

26 J. Huang, X. Zhao, X. Huang and W. Liang, Understanding the Mechanism of Plasmon-Driven Water Splitting: Hot Electron Injection and a near Field Enhancement Effect, *Phys. Chem. Chem. Phys.*, 2021, **23**(45), 25629–25636.

27 C. J. Herring and M. M. Montemore, Recent Advances in Real-Time Time-Dependent Density Functional Theory Simulations of Plasmonic Nanostructures and Plasmonic Photocatalysis, *ACS Nanosci. Au*, 2023, **3**(4), 269–279.

28 C. J. Herring and M. M. Montemore, Computational Discovery of Design Principles for Plasmon-Driven Bond Activation on Alloy Antenna Reactors, *ACS Nano*, 2025, **19**(10), 9860–9867.

29 M. Boronat, A. Leyva-Perez and A. Corma, Theoretical and Experimental Insights into the Origin of the Catalytic Activity of Subnanometric Gold Clusters: Attempts to Predict Reactivity with Clusters and Nanoparticles of Gold, *Acc. Chem. Res.*, 2014, **47**(3), 834–844.

30 P. Schwerdtfeger and M. Lein, Theoretical Chemistry of Gold–From Atoms to Molecules, Clusters, Surfaces and the Solid State. Gold Chem. Appl. Future Dir, *Life Sci.*, 2009, 183.

31 G. Kolesov, O. Grånäs, R. Hoyt, D. Vinichenko and E. Kaxiras, Real-Time TD-DFT with Classical Ion Dynamics: Methodology and Applications, *J. Chem. Theory Comput.*, 2016, **12**(2), 466–476.

32 M. M. Montemore, R. Hoyt, G. Kolesov and E. Kaxiras, Reaction-Induced Excitations and Their Effect on Surface Chemistry, *ACS Catal.*, 2018, **8**(11), 10358–10363.

33 Y. Zhang, T. Nelson, S. Tretiak, H. Guo and G. C. Schatz, Plasmonic Hot-Carrier-Mediated Tunable Photochemical Reactions, *ACS Nano*, 2018, **12**(8), 8415–8422.

34 J. P. Perdew, K. Burke and M. Ernzerhof, Generalized Gradient Approximation Made Simple, *Phys. Rev. Lett.*, 1996, **77**(18), 3865.

35 M. Chaudhary and H.-C. Weissker, Optical Spectra of Silver Clusters and Nanoparticles from 4 to 923 Atoms from the TDDFT+ U Method, *Nat. Commun.*, 2024, **15**(1), 9225.

36 C. J. Yocom, X. Zhang and Y. Liao, Research and Development Status of Laser Peen Forming: A Review, *Opt. Laser Technol.*, 2018, **108**, 32–45.

37 N. E. Koval, J. I. Juaristi and M. Alducin, Strong-Field Effects in the Photo-Induced Dissociation of the Hydrogen Molecule on a Silver Nanoshell, *Chem. Sci.*, 2024, **15**(44), 18581–18591.

38 D. Pal, D. Konar and B. S. Sumerlin, Poly(Vinyl Ketones): New Directions in Photodegradable Polymers, *Macromol. Rapid Commun.*, 2023, **44**(15), 2300126.

39 N. De Alwis Watuthanthrige, J. A. Reeves, M. T. Dolan, S. Valloppilly, M. B. Zanjani, Z. Ye and D. Konkolewicz, Wavelength-Controlled Synthesis and Degradation of Thermoplastic Elastomers Based on Intrinsically Photoresponsive Phenyl Vinyl Ketone, *Macromolecules*, 2020, **53**(13), 5199–5207.

40 Y. I. Derikov, D. R. Belousov, A. V. Finko, G. A. Shandryuk, N. M. Kuz'menok, S. G. Mikhalyonok, V. S. Bezborodov, E. V. Chernikova and R. V. Talroze, Novel Mesogenic Vinyl Ketone Monomers and Their Based Polymers, *Polymers*, 2022, **15**(1), 5.

41 X. F. Yao, D. L. Liu and H. Y. Yeh, Mechanical Properties and Gradient Variations of Polymers under Ultraviolet Radiation, *J. Appl. Polym. Sci.*, 2007, **106**(5), 3253–3258.

42 Z. Arslan, H. C. Kiliclar and Y. Yagci, Visible Light Induced Degradation of Poly(Methyl Methacrylate-*co*-methyl A-chloro Acrylate) Copolymer at Ambient Temperature, *Macromol. Rapid Commun.*, 2023, **44**(9), 2300066.

